Published in "Physical Chemistry Chemical Physics 18(19): 13196–13208, 2016"
which should be cited to refer to this work.

Photoluminescence properties of Yb^{2+} ions doped in the perovskites $CsCaX_3$ and $CsSrX_3$ (X = Cl, Br, and I) – a comparative study†

Markus Suta,[a] Werner Urland,[b] Claude Daul[b] and Claudia Wickleder*[a]

The Yb^{2+}-doped perovskite derivatives $CsMX_3$ (M = Ca and Sr; X = Cl, Br, and I) are ideal systems for obtaining a detailed insight into the structure–luminescence relationship of divalent lanthanides. The investigation of the respective photoluminescence properties yielded two emission bands in the violet and blue spectral range for all compounds, which are assigned to the spin-allowed and spin-forbidden 5d–4f transitions, respectively. The impact on their energetic positions is dependent on both the covalency of the Yb^{2+}-halide bond and the corresponding bond length in agreement with expectations. The excitation spectra provide a detailed fine structure at low temperatures and can be partly interpreted separating the $4f^{13}$ core from the 5d electron in the excited state. The local crystal field in $CsSrI_3$:Yb^{2+} provides a special case due to the trigonal distortion induced by the crystal structure that is clearly evident in the luminescence features of Yb^{2+}. The structure–property relationship of several spectroscopic key quantities of Yb^{2+} in this series of halides is analyzed in detail and parallels the properties of Eu^{2+} ions doped in the given perovskites.

1 Introduction

The photoluminescence properties of divalent lanthanides have attracted a lot of attention both from theoretical and applicational perspectives due to the parity-allowed character of the 5d–4f transitions they exhibit in the UV and visible range. Among them, Eu^{2+} is by far the most studied ion due to its rather high stability and the fact that it shows luminescence in essentially any visible color solely dependent on the appropriate choice of the respective host compound. A nice overview of the photoluminescence of many Eu^{2+}-activated compounds was given by Dorenbos,[1] while we recently presented a review of the luminescence properties of Eu^{2+}-doped nanoparticles.[2] In contrast, the luminescence properties of other divalent lanthanides are reported to a much lesser extent and basically limited to Sm^{2+}, Tm^{2+} and Yb^{2+}. Rubio reviewed the electronic spectra of Sm^{2+}, Eu^{2+} and Yb^{2+} in mainly alkali halides up to 1991,[3] whereas other representative examples of the luminescence of Sm^{2+} and Tm^{2+} in halides were reported for $MZnCl_4$ (M = Sr and Ba)[4] and $CsCaX_3$ (X = Cl, Br, and I).[5,6] Tm^{2+} is also known to show upconversion in halides.[7,8] In particular, the relatively low number of literature studies on the photoluminescence of Yb^{2+} and other divalent lanthanide ions compared to Eu^{2+} is mainly due to the high preparative challenge in stabilizing these ions in inorganic compounds.

Yb^{2+} exhibits a closed-shell $4f^{14}$ configuration in its ground state and hence it is also stabilized in many solids. Contrary to the case of Eu^{2+}, however, its luminescence is often quenched or related to excitonic features due to the proximity of the excited states to the conduction band of the respective host compound.[9,10] This extraordinary behavior is known as anomalous luminescence and has been recently investigated in much detail in fluorides where exciton trapping is often encountered.[11–13]

Due to its closed-shell ground state configuration, Yb^{2+} only shows broad-band 5d–4f luminescence from an excited $4f^{13}5d^1$ configuration, which is electric-dipole allowed for the free ion, and no 4f–4f emission. Although the respective emission bands are at very similar energies compared to those of Eu^{2+} in a given host, Yb^{2+} may show two emission bands due to the fact that it exhibits a more than half-filled ground state configuration. This is related to the fact that the lowest energetic excitation occurs under reversal of spin, which is termed as a spin-forbidden or high-spin (HS) transition. The corresponding spin-allowed or low-spin (LS) transition lies at higher energies according to Hund's rules. This special behavior has been shown very illustratively for the 4f ↔ 5d transitions of the heavy trivalent lanthanides in the VUV region.[14–16]

[a] Inorganic Chemistry, Faculty of Science and Technology, University of Siegen, Adolf-Reichwein-Str. 2, 57068 Siegen, Germany. E-mail: wickleder@chemie.uni-siegen.de; Fax: +49-271-7402555; Tel: +49-271-7404217
[b] Department of Chemistry, University of Fribourg, Chemin du Musée 9, 1700 Fribourg, Switzerland

† Electronic supplementary information (ESI) available: X-ray powder diffraction patterns of the presented Yb^{2+}-doped compounds. See DOI: 10.1039/c6cp00085a

The photoluminescence of Yb^{2+} had already been investigated in detail in selected alkaline-earth halides such as MgF_2,[17,18] CaF_2,[19] $SrCl_2$[20–22] or fluorohalides.[23] Another largely investigated class of compounds are Yb^{2+}-activated alkali halides.[24] In the cases of $SrCl_2$:Yb^{2+} [22] and NaCl:Yb^{2+},[25] both spin-forbidden and spin-allowed emissions are observed as expected. It was found that they show a sensitive temperature-dependent intensity variation of the emission transitions indicating a phonon-assisted population mechanism of the excited states. In fact, this phenomenon has been so far only rarely observed for Yb^{2+}. Besides halides, other materials have also been investigated. Among them are borates,[26] haloborates,[27] sulfates,[28] phosphates[29] or nitridosilicate-based host materials[30,31] to mention a few. Dorenbos also summarized the reported Yb^{2+}-doped compounds up to 2003,[32] where it is also revealed that halides form the largest class of investigated compounds so far.

Due to the small number of only 140 microstates in the excited $4f^{13}5d^1$ configuration, many calculations have been attempted on high-symmetry sites occupied by Yb^{2+} in halides. Most of them include semi-empirical crystal-field approaches with parameters fitted to the experimental spectra, as in the case of alkali halides[24] or $SrCl_2$.[22] More recently, Sánchez-Sanz *et al.* have reported about *ab initio* wavefunction-based relativistic calculations also including the low-lying excited $4f^{13}6s$ states for Yb^{2+} embedded in $SrCl_2$[33,34] and $CsCaBr_3$.[35–37]

Unlike the binary halides, the luminescence of Yb^{2+} in perovskite-analogue halides has been so far considered only for selected fluorides,[38] $RbCaCl_3$[39] and the purely Yb^{2+}-based iodides $AYbI_3$ (A = K, Rb, and Cs).[40] As recent publications show, especially Yb^{2+}-doped iodides have become interesting as potential new scintillating materials.[41–43] Based on the previously mentioned reasons, we therefore present a systematic analysis of the photoluminescence properties of Yb^{2+} doped into the perovskite-derivatives $CsMX_3$ (M = Ca and Sr, X = Cl, Br and I) that provide high-symmetry sites for Yb^{2+}. These compounds may be interesting as an experimental standard for theoretical models of the electronic structure of Yb^{2+} and as potential novel scintillators in accordance with the respective Eu^{2+}-doped compounds.[44–49] The photoluminescence properties of Eu^{2+} have already been reported in these compounds[44–52] which also allows a comparison between the spectroscopic properties of both divalent lanthanides.

2 Experimental

2.1 Preparation

For the preparation of the presented host compounds, the respective cesium halides CsCl (Merck, 99.5%), CsBr (Chempur, 99.9%) and CsI (Merck, 99.5%) were used. As an alkaline earth source, the respective hydrates $CaCl_2{\cdot}2H_2O$ (Merck, 99.5%), $SrCl_2{\cdot}6H_2O$ (Riedel de-Häen, 99+%), $CaBr_2{\cdot}6H_2O$ (Riedel de Häen, 99+%), $SrBr_2{\cdot}6H_2O$ (Alfa Aesar, 99%), $CaI_2{\cdot}4H_2O$ (Acros Organics, 99%) and SrI_2 (Heraeus, 99.9%) have been employed. All starting materials were pre-dried in a dynamic vacuum at 200 °C overnight, respectively, to remove all water contents. The hydrated iodides had been previously dissolved in diluted HI (Acros Organics, 57 wt%) to remove traces of residual carbonates that form upon standing of the hydrate in air. The Yb(II) halides YbX_2 (X = Cl, Br, and I) were obtained in good yields (~80–85%) by dissolution of the pre-dried desired ammonium halides NH_4Cl (Th. Geyer, 99.99%), NH_4Br (Alfa Aesar, 99.99%) and NH_4I (Riedel de-Häen, 99.9%), respectively, in liquified NH_3 (Messer, 99.999%) at −60 °C and addition of Yb metal (smart-elements, 99.999%) using the Schlenk technique.[53] In all cases, an orange-colored solid precipitated that changed its color to greenish-yellow upon evaporation of NH_3. The thus obtained intermediate $YbX_2{\cdot}xNH_3$ (X = Cl, Br, and I) was finally decomposed under vacuum at 250 °C for 3 h in each case and afforded the desired Yb(II) halide ranging from faint green ($YbCl_2$) over slight yellow ($YbBr_2$) to an intense yellow color (YbI_2). All starting materials have been checked for their purity by X-ray powder diffraction (XRD) (Stoe Stadi P, Cu K_α radiation).

The Yb^{2+}-doped host compounds were prepared by usage of the Bridgman technique fusing the respective halides CsX and MX_2 (M = Ca and Sr; X = Cl, Br, and I) in stoichiometric amounts together with 0.1 mol% YbX_2 (X = Cl, Br, and I) in sealed evacuated silica ampoules. The ampoules had been graphitized inside before by pyrolysis of acetone in order to avoid the contact of the Yb(II) halide with the glass at higher temperatures that leads to oxidation to the respective trivalent halide. All mixtures were heated at a rate of 20 °C h^{-1} to temperatures higher than their melting points and kept in the melt for 36 h.[54–56] After this, they were slowly cooled (2 °C h^{-1}) to 100 °C below their melting points in order to provide good crystallinity of the desired products. Finally, the mixtures were cooled down to room temperature with a cooling rate of 10 °C h^{-1}. The phase purity of all obtained Yb^{2+}-doped compounds was verified by XRD (see ESI†). Due to the high oxidation sensitivity of Yb^{2+} to moisture and air and the hygroscopic nature of the host compounds, all preparative steps were performed under dry Ar atmosphere in a glove box (Braun).

2.2 Optical measurements

For photoluminescence measurements of the presented halides, only transparent and clear pieces (~1 mm^3) of the obtained products were used. The photoluminescence emission and excitation spectra of the presented Yb^{2+}-doped halides were recorded on a Fluorolog3 spectrofluorometer (Horiba Jobin Yvon) equipped with a 450 W Xe lamp, double Czerny–Turner monochromators allowing a resolution down to 0.05 nm and a photomultiplier detection system R928P (Hamamatsu) with a photon counting system. The emission spectra were corrected for the photomultiplier sensitivity and the excitation spectra for the lamp intensity with the aid of a rhodamine 6G standard. All presented spectra were detected at 10 K by usage of a liquid He closed-cycle cryostat (Janis).

3 Results

3.1 Crystal structures and coordination spheres of Yb^{2+} in $CsMX_3$ (M = Ca and Sr; X = Cl, Br, and I)

The crystal structures of the host compounds have already been reported in detail in the literature.[54–56] It is known that Eu^{2+}

occupies the alkaline earth sites in these compounds, which are all 6-fold coordinated by the respective halide anions, as has been discussed by us for the respective bromides and iodides.[51,52] Hence, it is even more probable for Yb^{2+} ions to occupy the same sites ($r(Ca^{2+})$ = 1.00 Å, $r(Sr^{2+})$ = 1.18 Å for CN = 6)[57] due to their lower ionic radius compared to Eu^{2+} ions ($r(Eu^{2+})$ = 1.17 Å, $r(Yb^{2+})$ = 1.01 Å for CN = 6).[57] The occupation of the Cs^+ sites can be excluded, as they provide higher coordination numbers than 6 in all halides regarded in this paper (namely CN = 12 in $CsCaCl_3$, $CsCaBr_3$ and $CsSrCl_3$; CN = 10 for $CsCaI_3$ and $CsSrBr_3$ and CN = 8 for $CsSrI_3$) and thus differ significantly in both charge and size ($r(Cs^+) > 1.67$ Å for CN > 6) from Yb^{2+}.[57]

$CsCaCl_3$ and $CsCaBr_3$ both crystallize in a perfect cubic perovskite structure with the space group $Pm\bar{3}m$ (no. 221).[54,55] The coordination spheres of the 6-fold coordinated Ca^{2+} ions are perfectly octahedral and therefore provide highly symmetric O_h sites for the Yb^{2+} ions. The average distances of the Ca–Cl and Ca–Br bonds are 2.70 Å and 2.85 Å, respectively,[54,55] that can be assumed to remain undistorted upon doping with Yb^{2+} due to the similar sizes of both cations.[57] Both compounds are known to show phase transitions into a tetragonal phase with local C_{4v} symmetry at the Ca^{2+} sites in the case of $CsCaCl_3$[58] and into an orthorhombic phase with local C_i symmetry at the Ca^{2+} sites in the case of $CsCaBr_3$[55] at low temperatures. $CsSrCl_3$ crystallizes in a tetragonally distorted variant of a perovskite with the space group *P4mm* (no. 99) isostructural to $CsPbCl_3$.[54] The Sr^{2+} sites with an average Sr–Cl distance of 2.80 Å are coordinated in the form of tetragonally elongated octahedra with local C_{4v} symmetry. $CsCaI_3$ and $CsSrBr_3$ crystallize isostructurally in a $GdFeO_3$-type structure with the space group *Pnma* (no. 62).[56] Both alkaline earth sites are coordinated in an octahedral fashion by 6 halide ions, respectively, with local C_i symmetry. The octahedra are slightly tilted towards each other in this structure type. The average Sr–Br distance is 2.98 Å, whereas the average Ca–I distance is 3.10 Å.[56] Finally, $CsSrI_3$ crystallizes in a filled $PuBr_3$ type structure with the space group *Cmcm* (no. 63).[56] The coordination spheres of the Sr^{2+} ions with local C_{2h} site symmetry are also of octahedral fashion. However, the octahedra are highly tilted towards each other in this structure inducing a trigonal distortion. The average Sr–I distance is 3.37 Å in this compound. An approximation by O_h symmetry has been recently shown to fail for the interpretation of the photoluminescence spectra of Eu^{2+} in $CsSrI_3$,[52] whereas for the other compounds, O_h is a valid approximation.[51,52] Hence, it is expected to observe similar effects for the spectra of Yb^{2+}, which will be discussed below. For more details and pictures of the previously described coordination spheres, we refer to the literature and references mentioned therein.[51,52,54,56]

3.2 Photoluminescence spectra of $CsMX_3$:Yb^{2+} (M = Ca and Sr; X = Cl, Br, and I)

All the presented Yb^{2+}-doped halides $CsMX_3$ (M = Ca and Sr; X = Cl, Br, and I) show bright blue luminescence upon UV irradiation at room temperature. All presented spectra were detected at 10 K due to the much higher resolution that allows very clear interpretations.

Throughout this paper, we employ the crude approximation of a decoupled strong-field scheme for the interpretation, in which the 4f electrons are treated separately from the excited 5d electron. Hence, the 4f orbitals are treated as quasi-free and characterized by their respective term symbols in the LS coupling scheme, whereas the 5d orbitals are more prone to the ligand field and hence experience the effect of the crystal field to first order. We have already shown for the respective Eu^{2+}-doped compounds that this approximation is useful for interpretation of the spectra.[51,52] The presence of a well-resolved fine structure of the divalent lanthanides indicates a weak Coulomb interaction between the 4f and 5d electrons.[59] It should be mentioned, however, that this approach is only a first-order approximation and the Coulomb interaction can in fact not be neglected for a correct assignment of the excited states. This has been nicely shown in the cases of $CsCaBr_3$:Ln^{2+} (Ln = Yb and Eu)[35,60] and $CsMgBr_3$:Eu^{2+}[61] by different theoretical approaches very recently. Nonetheless, from a spectroscopic point of view, this crude approximation is particularly useful to extract parameters such as the crystal field splitting and the Stokes shift without detailed calculations.

3.2.1 $CsMCl_3$:0.1% Yb^{2+} (M = Ca and Sr). The luminescence spectra of Yb^{2+}-doped $CsCaCl_3$ and $CsSrCl_3$ are depicted in Fig. 1. In both compounds, two emission bands in the violet and blue range are observed at 10 K, respectively. For $CsCaCl_3$:Yb^{2+}, the dominant emission band located at 22 600 cm^{-1} (442 nm) only shows a slight asymmetry with a full width at half maximum (FWHM) of Γ_{HS}(10 K) = 690 cm^{-1}. It can be assigned to the spin-forbidden transition $4f^{13}(^2F_{7/2})5d^1(t_{2g}, HS) \rightarrow 4f^{14}(^1S_0)$ of Yb^{2+} substituting the octahedrally coordinated Ca^{2+} sites. The emission band at 24 320 cm^{-1} (411 nm) is assigned to the respective spin-allowed transition $4f^{13}(^2F_{7/2})5d^1(t_{2g}, LS) \rightarrow 4f^{14}(^1S_0)$ of Yb^{2+}. The FWHM of the spin-allowed transition at 10 K is found to have the value of Γ_{LS}(10 K) = 900 cm^{-1}. Both emission bands are separated by the effect of exchange interaction and have an energetic difference of ΔE_{exch} = 1720 cm^{-1}, in a reasonable order of magnitude compared to the values found for other chlorides such as $SrCl_2$:Yb^{2+} (2090 cm^{-1})[20,21] or NaCl:Yb^{2+} (1960 cm^{-1}).[25] Especially in the case of NaCl:Yb^{2+}, also very similar emission energies are found compared to $CsCaCl_3$:Yb^{2+}, which seems plausible due to the similarity in ionic radii of Na^+ ($r(Na^+)$ = 1.02 Å for CN = 6) and Ca^{2+} ($r(Ca^{2+})$ = 1.00 Å for CN = 6).[57] In $RbCaCl_3$:Yb^{2+}, the dominant emission was reported to be located at 22 830 cm^{-1} (438 nm) at room temperature, which also fits nicely into expectations.[39]

The photoluminescence excitation spectrum of $CsCaCl_3$:Yb^{2+} (see Fig. 1(a)) provides a distinct fine structure that can be partly interpreted within the approximation of a decoupled scheme as explained above. Its general appearance is very similar to the excitation spectra reported for Yb^{2+}-activated sodium and potassium halides.[24] Basically, three groups of bands can be identified that are assigned to the transitions $4f^{14}(^1S_0) \rightarrow 4f^{13}(^2F_{7/2})5d^1(t_{2g})$, $4f^{13}(^2F_{5/2})5d^1(t_{2g})$ and $4f^{13}(^2F_{7/2})5d^1(e_g)$ in the order of increasing energy (see Fig. 1(a)). The first dominant band at 25 200 cm^{-1} (397 nm) is assigned to the spin-allowed transition $4f^{14}(^1S_0) \rightarrow 4f^{13}(^2F_{7/2})5d^1(t_{2g}, LS)$, whereas the corresponding HS transition

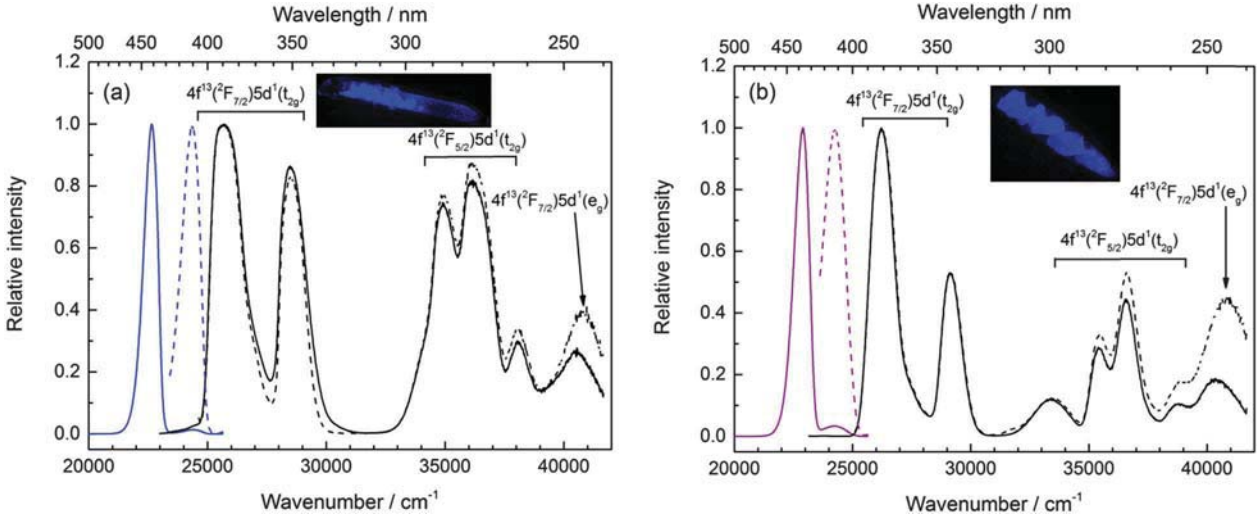

Fig. 1 (a) Photoluminescence excitation (black, solid: E_{em} = 22 630 cm^{-1} (HS), dashed: E_{em} = 24 390 cm^{-1} (LS)) and emission spectra (blue; solid: HS emission; dashed: LS emission, both excited at E_{ex} = 25 910 cm^{-1}) of $CsCaCl_3$:0.1% Yb^{2+} at 10 K. (b) Photoluminescence excitation (black, solid: E_{em} = 22 880 cm^{-1} (HS), dashed: E_{em} = 24 390 cm^{-1} (LS)) and emission spectra (violet; solid: HS emission; dashed: LS emission, both excited at E_{ex} = 26 320 cm^{-1}) $CsSrCl_3$:0.1% Yb^{2+} at 10 K. Insets: Photographs indicating the photoluminescence of the Yb^{2+}-doped samples upon UV irradiation at room temperature.

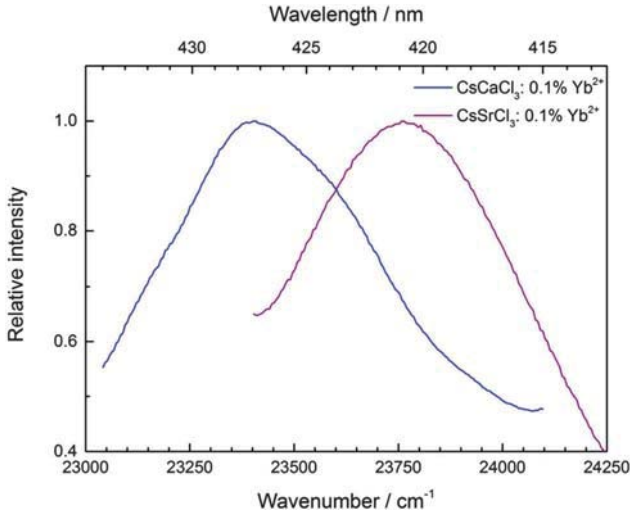

Fig. 2 Photoluminescence excitation spectra recorded at 10 K indicating the presence of the first spin-forbidden transitions $4f^{14}(^1S_0) \rightarrow 4f^{13}(^2F_{7/2})5d^1(t_{2g}, HS)$ in $CsCaCl_3$:Yb^{2+} (blue, E_{em} = 22 730 cm^{-1}) and $CsSrCl_3$:Yb^{2+} (violet, E_{em} = 22 880 cm^{-1}).

is depicted in Fig. 2 and located at 23 430 cm^{-1} (427 nm). A summary of the most important spectroscopic properties deduced from the photoluminescence spectra is provided in Table 1.

The first two groups of bands have an energetic difference of 9770 cm^{-1} on average, in accordance with the expectations from the Dieke diagram for Yb^{3+}.[62] This makes the assignments plausible. The third group is assigned to excitations into the e_g orbitals (see Fig. 1) and thus allows an experimental estimation of the crystal field splitting of 10 Dq = 14 030 cm^{-1} in the case of $CsCaCl_3$:Yb^{2+}. This is in reasonable good agreement with the values found for NaCl:Yb^{2+} between 12 000 cm^{-1} [63] and 13 600 cm^{-1},[24,64] in which a similar Yb–Cl distance is given for the O_h-symmetric crystal field.

Table 1 Deduced spectroscopic properties of Yb^{2+} doped in $CsMCl_3$ (M = Ca and Sr). All energies are in cm^{-1}

	$CsCaCl_3$:Yb^{2+}	$CsSrCl_3$:Yb^{2+}
Stokes shift ΔS_{HS}	830	920
Stokes shift ΔS_{LS}	890	1670
HS–LS splitting ΔE_{exch}[a]	1745	1990
Spin–orbit splitting ΔE_{so}	9770	10 040
Crystal field splitting 10 Dq	14 030	13 380

[a] Averaged values from emission and excitation spectra.

The possibility for a clear assignment of the first excited states allows a quite precise determination of the Stokes shift. Based on these assignments, a Stokes shift of ΔS_{HS} = 830 cm^{-1} is found for the spin-forbidden transition in the case of $CsCaCl_3$:Yb^{2+}, whereas a Stokes shift of ΔS_{LS} = 890 cm^{-1} is deduced for the respective spin-allowed transition $4f^{14}(^1S_0) \rightarrow 4f^{13}(^2F_{7/2})5d^1(t_{2g}, LS)$, which is located at 25 200 cm^{-1} at 10 K (see Fig. 1(a)). The energetic difference between the HS and LS excitation bands is 1770 cm^{-1}, in close agreement with the difference found from the emission spectra. Both Stokes shifts are very small, in good agreement with the respective low FWHMs. The HS and LS assignments should, however, be made with caution, as calculations on $CsCaBr_3$:Yb^{2+} have indicated that the spin character of these excited states is not totally pure in nature.[35,36] Especially in the excitation spectrum obtained upon detection of the HS emission (see the solid curve in Fig. 1(a)), it is evident that the excited states at higher energies have a much stronger influence on this emission.

$CsSrCl_3$:Yb^{2+} shows similar emission spectra at 10 K (see Fig. 1(b)). Like in the case of $CsCaCl_3$, a dominant spin-forbidden emission located at 22 880 cm^{-1} (437 nm) at 10 K is detected that is due to the transition $4f^{13}(^2F_{7/2})5d^1(t_{2g}, HS) \rightarrow 4f^{14}(^1S_0)$. It shows an asymmetry, which is most probably due to the

mismatch of the ionic radii of Sr^{2+} and Yb^{2+} (see Section 3.1)[57] as well as due to the tetragonally distorted symmetry to C_{4v}. This is also apparent on the slightly larger FWHM of the HS emission with respect to the Ca-based compound, namely $\Gamma_{HS}(10\ K) = 740\ cm^{-1}$. The respective spin-allowed transition $4f^{13}(^2F_{7/2})5d^1(t_{2g}, LS) \rightarrow 4f^{14}(^1S_0)$ is located at 24 340 cm^{-1} (411 nm) at 10 K. The FWHM of the LS emission is larger than for the respective HS transition and reads $\Gamma_{LS}(10\ K) = 1230\ cm^{-1}$. The larger values of the FWHMs of the emission bands in Yb^{2+}-doped $CsSrCl_3$ already indicate a stronger vibrational interaction which is also confirmed by the larger Stokes shifts of $\Delta S_{HS} = 920\ cm^{-1}$ and $\Delta S_{LS} = 1670\ cm^{-1}$ at 10 K. This also seems plausible by the argument of size differences in the ionic radii of Sr^{2+} and Yb^{2+}. The energetic difference of the HS and LS emission bands is 1865 cm^{-1} in this case. In the excitation spectrum, however, the respective average difference between the two lowest energy transitions is somewhat larger with 2110 cm^{-1}, in very good agreement with the value reported for $SrCl_2:Yb^{2+}$ (2090 cm^{-1}).[20,21] The excitation spectrum of $CsSrCl_3:Yb^{2+}$ (see Fig. 1(b)) is characterized by a very similar fine structure as the respective spectrum of $CsCaCl_3:Yb^{2+}$ and can also be subdivided into three groups that are assigned to the transitions $4f^{14}(^1S_0) \rightarrow 4f^{13}(^2F_{7/2})5d^1(t_{2g})$, $4f^{13}(^2F_{5/2})5d^1(t_{2g})$ and $4f^{13}(^2F_{7/2})5d^1(e_g)$ in the order of increasing energy within the decoupled scheme.

The first and second group of excitation bands also have an average energetic distance of 10 040 cm^{-1} again characteristic of the separation of the spin–orbit split terms of the $4f^{13}$ core in the excited state.[62] Based on the assignments made, a crystal field splitting of 10 Dq = 13 380 cm^{-1} was determined from the spectra. It is slightly smaller than the value found for $CsCaCl_3:Yb^{2+}$, which is reasonable taking into account the larger Yb–Cl distances in $CsSrCl_3:Yb^{2+}$. Moreover, the value is in close agreement with the experimentally determined crystal field splitting reported for $SrCl_2:Yb^{2+}$ (10 Dq = 13 600 cm^{-1}).[21]

Fig. 2 also reveals the presence of a low-intensity excitation band located at 23 760 cm^{-1} (421 nm) that can be assigned to the spin-forbidden transition $4f^{14}(^1S_0) \rightarrow 4f^{13}(^2F_{7/2})5d^1(t_{2g}, HS)$. This is in complete analogy to $CsCaCl_3:Yb^{2+}$. However, no additional fine structure is observed for this band, although a descent in symmetry should be expected due to the given lower site symmetry of C_{4v} as well as the mismatch in the ionic radii between Yb^{2+} and Sr^{2+} in this material. The respective spin-allowed transition $4f^{14}(^1S_0) \rightarrow 4f^{13}(^2F_{7/2})5d^1(t_{2g}, LS)$ is located at 25 870 cm^{-1} (387 nm), as evident from Fig. 1(b).

Some important spectroscopic quantities deduced from the spectra of $CsMCl_3:Yb^{2+}$ (M = Ca and Sr) are summarized in Table 1.

In both chlorides, the spin-forbidden emission is highly dominant even upon excitation into the respective LS state. This indicates a strong multiphonon relaxation even at 10 K, which will be regarded by us in future.

3.2.2 $CsMBr_3$:0.1% Yb^{2+} (M = Ca and Sr). Like the chlorides, the Yb^{2+}-activated bromides $CsMBr_3$ (M = Ca and Sr) show two emission bands in the violet and blue range, respectively. Their spectra are depicted in Fig. 3(a) and (b), whereas the most important spectroscopic parameters are compiled in Table 2.

The dominant violet emission band in $CsCaBr_3:Yb^{2+}$ at 10 K (see Fig. 3(a), dashed blue curve) shows a slight asymmetry and is located at 24 310 cm^{-1} (411 nm). It can be assigned to the spin-allowed transition $4f^{13}(^2F_{7/2})5d^1(t_{2g}, LS) \rightarrow 4f^{14}(^1S_0)$ and has a FWHM of $\Gamma_{LS}(10\ K) = 770\ cm^{-1}$.

The respective spin-forbidden emission $4f^{13}(^2F_{7/2})5d^1(t_{2g}, HS) \rightarrow 4f^{14}(^1S_0)$ shows a maximum at 22 630 cm^{-1} (442 nm) and becomes only very strong upon selective excitation (E_{ex} = 25 770 cm^{-1}) at 10 K. The FWHM of this emission is also low with $\Gamma_{HS}(10\ K) = 850\ cm^{-1}$. The Stokes shifts of the Yb^{2+}-related emissions in this compound are $\Delta S_{HS} = 970\ cm^{-1}$ and $\Delta S_{LS} = 960\ cm^{-1}$ at 10 K, respectively. Moreover, the emission bands are almost at

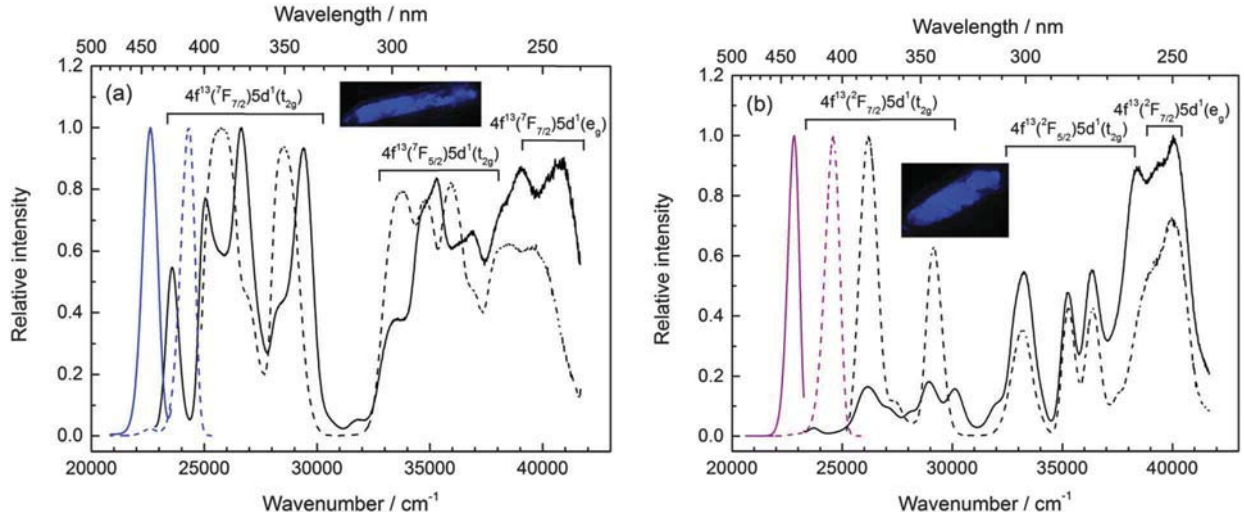

Fig. 3 (a) Photoluminescence excitation (black, solid: E_{em} = 22 570 cm^{-1} (HS), dashed: E_{em} = 24 690 cm^{-1} (LS)) and emission spectra (blue; solid: HS emission, E_{ex} = 25 770 cm^{-1}; dashed: LS emission, E_{ex} = 25 770 cm^{-1}) of $CsCaBr_3$:0.1% Yb^{2+} at 10 K. (b) Photoluminescence excitation (black, solid: E_{em} = 22 730 cm^{-1} (HS), dashed: E_{em} = 24 690 cm^{-1} (LS)) and emission spectra (violet; solid: HS emission, E_{ex} = 23 670 cm^{-1}; dashed: LS emission, E_{ex} = 26 320 cm^{-1}) of $CsSrBr_3$:0.1% Yb^{2+} at 10 K. Insets: photographs indicating the photoluminescence of the Yb^{2+}-doped samples upon UV irradiation at room temperature.

Table 2 Deduced spectroscopic properties of Yb^{2+} doped in $CsMBr_3$ (M = Ca and Sr). All energies are in cm^{-1}

	$CsCaBr_3:Yb^{2+}$	$CsSrBr_3:Yb^{2+}$
Stokes shift ΔS_{HS}	970	920
Stokes shift ΔS_{LS}	960	1510
HS–LS splitting ΔE_{exch}[a]	1670	2070
Spin–orbit splitting ΔE_{so}	9500	9280
Crystal field splitting 10 Dq	13 060	12 420

[a] Averaged values from emission and excitation spectra.

the same positions as in the case of $CsCaCl_3:Yb^{2+}$, which is a result of compensation between the nephelauxetic effect and the crystal field splitting 10 Dq (see also Section 4). In the photoluminescence excitation spectra of $CsCaBr_3:Yb^{2+}$ (see Fig. 3(a)), the well-resolved fine structure is again evident and can be interpreted in terms of the previously mentioned decoupled scheme. The energetic difference between the first two groups of bands is 9500 cm^{-1} in close agreement with the difference between the $^2F_{7/2}$ and $^2F_{5/2}$ levels of Yb^{3+} according to the Dieke diagram.[62] The additional fine structure may only be interpreted properly with more profound schemes (see Section 4). Based on the made assignments, a crystal field splitting of 10 Dq = 13 060 cm^{-1} can be estimated from the spectra. The crystal field splitting is lower than in the case of $CsCaCl_3:Yb^{2+}$ (see Table 1) and is in reasonable order of magnitude compared to the values found for $CsCaBr_3:Eu^{2+}$ (10 Dq = 11 550–12 700 cm^{-1})[51,60] or $NaBr:Yb^{2+}$ (10 Dq = 11 800 cm^{-1}).[24,64] *Ab initio* calculations available on $CsCaBr_3:Yb^{2+}$ slightly overestimate the crystal field splitting (10 Dq = 16 760–18 935 cm^{-1}), which is mainly assigned to the fact that the calculations are based on a shorter Yb–Br bond length.[36,37]

As already indicated for the chlorides, the first two excitation bands are the spin-forbidden and spin-allowed $4f^{14}(^1S_0) \rightarrow 4f^{13}(^2F_{7/2})5d^1(t_{2g}$, HS/LS) transitions (see Fig. 3(a)), respectively, which have an energy distance of 1675 cm^{-1}. The respective energetic difference between the emission bands averaged for both temperatures is 1670 cm^{-1} and in the range of the value found for Yb^{2+} in $CsCaCl_3$ and NaCl.[25] This highly justifies the attempted assignments.

Fig. 3(b) shows the detected photoluminescence spectra of Yb^{2+}-doped $CsSrBr_3$. Like in $CsCaBr_3$, a dominant, slightly asymmetric violet emission is present at 10 K, which is located at 24 550 cm^{-1} (407 nm). It is assigned to the spin-allowed transition $4f^{13}(^2F_{7/2})5d^1(t_{2g}$, LS) $\rightarrow 4f^{14}(^1S_0)$ and has a FWHM of Γ_{LS}(10 K) = 810 cm^{-1}. A blue emission is also detected at 22 780 cm^{-1} (439 nm) upon selective excitation. It arises due to the spin-forbidden transition $4f^{13}(^2F_{7/2})5d^1(t_{2g}$, HS) $\rightarrow 4f^{14}(^1S_0)$ of Yb^{2+}. The FWHM of this band is Γ_{HS}(10 K) = 680 cm^{-1} at 10 K. The emission energies are also very similar to the respective energies of Yb^{2+} doped in $CsSrCl_3$, again indicating the compensation of the nephelauxetic effect with the magnitude of the crystal field splitting 10 Dq (see Section 4). The Stokes shifts for the spin-forbidden and spin-allowed transitions are ΔS_{HS} = 920 cm^{-1} and ΔS_{LS} = 1510 cm^{-1}.

The photoluminescence excitation spectra also show a prominent fine structure as discussed for the previously described Yb^{2+}-doped compounds. The first two groups have an average energetic distance of 9280 cm^{-1} as expected from the energy difference of the $^2F_{7/2}$ and $^2F_{5/2}$ states of Yb^{3+}.[62] According to the assignments of the different excitation bands, the crystal field splitting is estimated to be 10 Dq = 12 420 cm^{-1}, which nicely fits into the expectations upon consideration of the respective metal–ligand distances when compared to $CsSrBr_3:Eu^{2+}$ (10 Dq = 11 860 cm^{-1})[51] or the reported values of $SrCl_2:Yb^{2+}$,[21] $NaBr:Yb^{2+}$ (see above)[24,64] or $KBr:Yb^{2+}$ (10 Dq = 10 800 cm^{-1}).[24,64] The first two excitation bands may again be assigned to the spin-forbidden and spin-allowed $4f^{14}(^1S_0) \rightarrow 4f^{13}(^2F_{7/2})5d^1(t_{2g}$, HS/LS) transitions located at 23 700 cm^{-1} and 26 060 cm^{-1}, respectively. Based on this, their energy splitting is 2360 cm^{-1}, which is slightly larger than the value found from the emission spectra (1780 cm^{-1}) similar to $CsSrCl_3:Yb^{2+}$.

3.2.3 $CsMI_3$:0.1% Yb^{2+} (M = Ca and Sr). The Yb^{2+}-doped iodides $CsMI_3$ (M = Ca and Sr) show bluish-violet luminescence upon UV irradiation at room temperature. Their photoluminescence spectra are depicted in Fig. 4(a) and (b). The most important deduced spectroscopic parameters can be found in Table 3.

A fairly symmetric Gaussian emission band readily recognized as the spin-allowed transition $4f^{13}(^2F_{7/2})5d^1(t_{2g}$, LS) $\rightarrow 4f^{14}(^1S_0)$ characterizes the emission spectrum of $CsCaI_3:Yb^{2+}$ (see Fig. 4(a), blue dashed curve). It is located at 23 420 cm^{-1} (427 nm) and has a FWHM of Γ_{LS}(10 K) = 700 cm^{-1}. The respective spin-forbidden emission $4f^{13}(^2F_{7/2})5d^1(t_{2g}$, HS) $\rightarrow 4f^{14}(^1S_0)$ is detected at 21 770 cm^{-1} (459 nm) and only dominant upon selective excitation (see Fig. 4(a), blue solid curve). The FWHM for the HS transition is Γ_{HS}(10 K) = 740 cm^{-1}. Based on this, the Stokes shifts of the Yb^{2+}-related emissions in this compound are ΔS_{HS} = 875 cm^{-1} and ΔS_{LS} = 1520 cm^{-1} at 10 K, respectively. Both emission bands are red-shifted compared to the Yb^{2+} emissions in $CsCaCl_3$ and $CsCaBr_3$, which is reasonable considering the higher covalency of the Yb–I bond and the respective larger influence of the nephelauxetic effect (see also Section 4).

Similar to the previously described materials, the excitation spectra reveal the presence of three groups that are readily interpreted within the decoupled scheme. An average energy difference of 9380 cm^{-1} between the $^2F_{7/2}$ and the $^2F_{5/2}$ submanifolds is estimated from the excitation spectra (see Fig. 4(a)), in reasonable agreement with expectations for the $4f^{13}$ core in the excited state.[62] Based on the attempted assignments, a crystal field splitting of 10 Dq = 11 830 cm^{-1} can be deduced that again nicely fits into the expectations since it is smaller than the values found for Yb^{2+} doped in $CsCaCl_3$ and $CsCaBr_3$ and is slightly larger than for Eu^{2+} in $CsCaI_3$ (10 Dq = 11 030 cm^{-1})[52] due to the smaller Yb–I bond length. More agreement is seen upon comparison with compounds with either similar covalency or slightly larger metal–ligand distances such as $NaI:Yb^{2+}$ (10 Dq = 9400–10 300 cm^{-1}) or with higher ionicity and similar bond lengths such as $KCl:Yb^{2+}$ (10 Dq = 12 400 cm^{-1}).[24,64] It is clearly seen that our found value ranges well with the reported crystal field splittings above. From the emission spectra, an energy of 1680 cm^{-1} may be deduced for the splitting between the first spin-forbidden and spin-allowed states. This coincides roughly

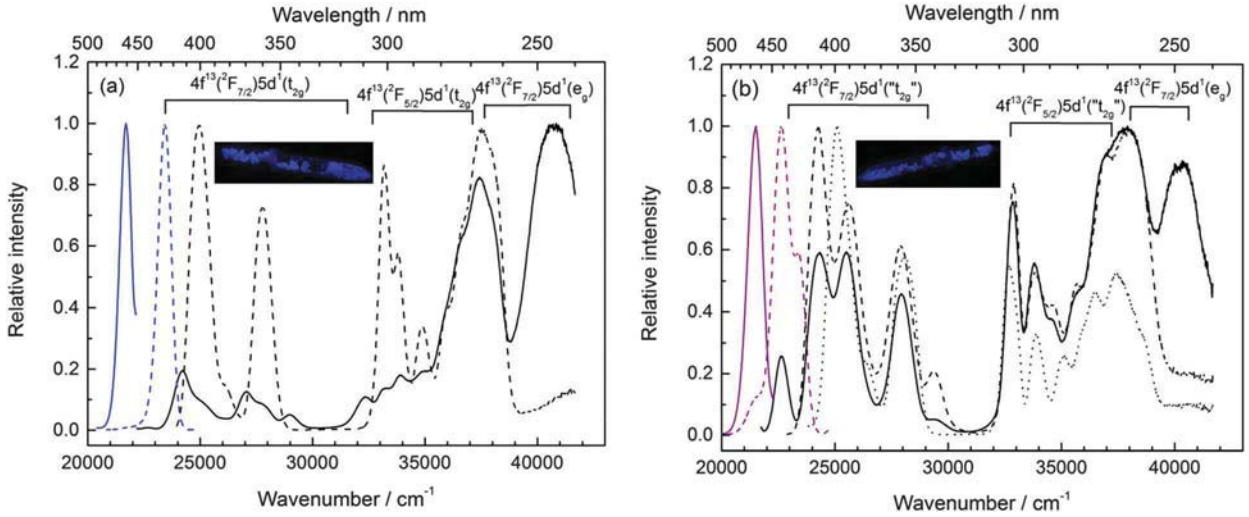

Fig. 4 (a) Photoluminescence excitation (black, solid: E_{em} = 21 830 cm^{-1} (HS), dashed: E_{em} = 23 360 cm^{-1} (LS)) and emission spectra (blue; solid: HS emission, E_{ex} = 22 730 cm^{-1}; dashed: LS emission, E_{ex} = 25 000 cm^{-1}) (blue) of $CsCaI_3$:0.1% Yb^{2+} at 10 K. (b) Photoluminescence excitation (black, solid: E_{em} = 21 505 cm^{-1} (HS), dashed: E_{em} = 22 470 cm^{-1} (LS1), dotted: E_{em} = 23 530 cm^{-1} (LS2)) and emission spectra (violet; solid: HS emission, E_{ex} = 22 730 cm^{-1}; dashed: LS emissions, E_{ex} = 25 000 cm^{-1}) of $CsSrI_3$:0.1% Yb^{2+} at 10 K. Insets: photographs indicating the photoluminescence of the Yb^{2+}-doped samples upon UV irradiation at room temperature.

Table 3 Deduced spectroscopic properties of Yb^{2+} doped in $CsMI_3$ (M = Ca and Sr). All energies are in cm^{-1}

	$CsCaI_3$:Yb^{2+}	$CsSrI_3$:Yb^{2+}
Stokes shift ΔS_{HS}	875	1140
Stokes shift ΔS_{LS}	1520	1550
HS–LS splitting ΔE_{exch}[a]	1795	1865
Spin–orbit splitting ΔE_{so}	9380	9850
Crystal field splitting 10 Dq	11 830	10 910

[a] Averaged values from emission and excitation spectra.

with the value found from the excitation spectrum (1910 cm^{-1}) and is in good agreement with the determined values in the other halides described so far in this paper.

The photoluminescence spectra of $CsSrI_3$:Yb^{2+} are depicted in Fig. 4(b). Contrary to the previously described doped compounds, Yb^{2+} shows three emission bands at 10 K in this compound. The low-energy emission located at 21 490 cm^{-1} (465 nm) at 10 K is the only one with a decay time in the ms range (not shown in this paper) thus allowing the formal assignment to the spin-forbidden transition $4f^{13}(^2F_{7/2})5d^1$(HS) → $4f^{14}(^1S_0)$. It should be noted that we omitted the designation of t_{2g} here, which will be clear from reasons explained below. The spin-forbidden emission can be selectively excited. Its FWHM at 10 K is Γ_{HS}(10 K) = 790 cm^{-1} and increases to 1760 cm^{-1} at room temperature. Its energy is slightly red-shifted compared to the respective transition of Yb^{2+} in $CsCaI_3$, which is easily explained if the trigonal distortion due to the strong tilt of the $[SrI_6]^{4-}$ octahedra in the crystal structure of $CsSrI_3$ is taken into account.[56] A similar effect was observed for the photoluminescence of Eu^{2+} doped into $CsSrI_3$ and intensively discussed by us.[52] One consequence is the splitting of the t_{2g} orbitals into a_{1g} and e_g orbitals within D_{3d} symmetry to the first order. This additional splitting leads to the observed red-shift of the respective spin-forbidden transition in $CsSrI_3$. The Stokes shift for this transition was determined with ΔS_{HS} = 1140 cm^{-1} at 10 K. The respective spin-forbidden excitation band shows little vibrational progression (not shown in Fig. 4(b)), which allows the determination of an average phonon energy of 130 cm^{-1}.

Two other emission bands can be detected in $CsSrI_3$:Yb^{2+} (see Fig. 4(b)) in contrast to the previously described phosphors. Both emission bands are characterised by decay times lower than 10 μs and are thus clearly identified as spin-allowed transitions $4f^{13}(^2F_{7/2})5d^1$(LS) → $4f^{14}(^1S_0)$ in the decoupled scheme. The lower energetic emission denoted as LS1 is located at 22 640 cm^{-1} (442 nm), whereas the higher energetic emission denoted as LS2 is present as a clearly resolved shoulder peaking at 23 480 cm^{-1} (426 nm). The fact that two emissions are observed here is another strong hint on a non-negligible trigonal distortion and shows that the emissive LS state is lifted in its degeneracy upon symmetry reduction to D_{3d}. The FWHMs of both the LS emissions read Γ_{LS1}(10 K) = 850 cm^{-1} and Γ_{LS2}(10 K) = 630 cm^{-1}, respectively. Both spin-allowed emissions show a Stokes shift of ΔS_{LS1} = 1540 cm^{-1} and ΔS_{LS2} = 1560 cm^{-1} to the corresponding excitation bands at 10 K, respectively. All emission bands are red-shifted compared to the corresponding emissions of Yb^{2+} in the previously discussed Sr-based halides, which is in good agreement with expectations according to the higher impact of the nephelauxetic effect. However, the emissions are also slightly red-shifted with respect to the corresponding emissions of Yb^{2+} in $CsCaI_3$, which is again a manifestation of the trigonal distortion of the Sr^{2+} sites in $CsSrI_3$. Another recent example suitable for comparison is SrI_2:Yb^{2+}, which has been reported to exhibit scintillation properties and shows the spin-allowed and the spin-forbidden emissions at 23 920 cm^{-1} (418 nm) and 22 420 cm^{-1} (446 nm), respectively, at room temperature.[43] The emission energies in $CsSrI_3$ fit well taking into account that the coordination number

of the Sr^{2+} sites in SrI_2 is higher than 6, and hence a slight blue-shift with respect to the emission of Yb^{2+} doped in the compound $CsSrI_3$ is expected.

Although slightly more complicated, the general structure of the excitation spectrum of $CsSrI_3$:Yb^{2+} (see Fig. 4(b)) is very similar to the previously described Yb^{2+}-doped compounds. The three groups of excitation bands with additional fine structure are evident and can be readily assigned according to the decoupled scheme. The first two groups have an average energy difference of 9850 cm^{-1} again in good agreement with the expectations for an Yb^{3+} core in the excited state.[62]

Upon detection of both spin-allowed emissions, two separate strong excitation bands located at 24 200 cm^{-1} (413 nm, LS1) and 25 020 cm^{-1} (400 nm, LS2) can be identified (see Fig. 4(b)) based on the transition $4f^{14}(^1S_0) \rightarrow 4f^{13}(^2F_{7/2})5d^1$(LS) that have the same energetic difference as the corresponding emission bands. This justifies our assignments. The respective excitation band for the spin-forbidden transition $4f^{14}(^1S_0) \rightarrow 4f^{13}(^2F_{7/2})5d^1$(HS) is, however, located at 22 650 cm^{-1}. If trigonal distortion is taken into account, the undistorted energy of the LS state in $CsSrI_3$ can be estimated from the known energies of the luminescence spectra to 24 750 cm^{-1}, whereas the corresponding emission would be located at 23 200 cm^{-1}. This is based on the fact that the LS state is triply degenerate in octahedral symmetry and splits into doubly and singly degenerate crystal field states in D_{3d} symmetry (see Section 4.2). The estimated energy of the undistorted LS state is then the resulting barycenter of the crystal field states in D_{3d}.

The preliminary considerations give rise to an estimated exchange splitting of 2020 cm^{-1} between the first spin-forbidden and spin-allowed states deduced from the excitation spectra. The respective splitting deduced from the emission spectra is somewhat lower with 1710 cm^{-1}. Both values are again very similar to the corresponding values found for Yb^{2+} doped in $CsSrCl_3$ and $CsSrBr_3$.

In spite of the trigonal distortion, it is possible to estimate the crystal field splitting for the undistorted case from the photoluminescence excitation spectra depicted in Fig. 4(b) (see above). We found a value of 10 Dq = 10 910 cm^{-1}, which looks reasonable as it is lower than the respective splittings deduced from $CsSrCl_3$ and $CsSrBr_3$ as well as $CsCaI_3$ and fits well into estimations reported for Eu^{2+} (10 Dq = 9600 cm^{-1}).[52]

4 Discussion

4.1 Photoluminescence of $CsMX_3$:Yb^{2+} (M = Ca and Sr; X = Cl, Br, and I)

Yb^{2+} shows very intense bluish-violet emission when doped into the halide-based perovskite-analogues $CsMX_3$ (M = Ca and Sr; X = Cl, Br, and I). The emission energies nicely fit into expectations upon comparison with other halides[20,22,24,43] In particular, the Yb^{2+}-related emission bands have energies very close to those of Eu^{2+} doped in the presented compounds[44–52] Unlike Eu^{2+}, however, Yb^{2+} shows both spin-forbidden and spin-allowed emissions in all compounds. This observation is in accordance with the estimations summarized by Dorenbos (see also eqn (1)–(4)) and indicates that the assumption of similar Stokes shifts and similar centroid shifts of Eu^{2+} and Yb^{2+} in the presented compounds is very well fulfilled.[32] In fact, these assumptions allow a very reliable estimation of the lowest excitation and emission energies of Yb^{2+} based on the known luminescence data from Eu^{2+} in these particular halides (see Table 4) according to the equations[32]

Table 4 Summary of the measured emission and excitation energies (10 K) of Yb^{2+} doped in $CsMX_3$ (M = Ca and Sr; X = Cl, Br, and I) and the estimated values according to the luminescence data for Eu^{2+}.[44–52] All energies are in cm^{-1}

	Experimental data described in this work			
Compound	E_{ex}(14, 2+, A, LS)	E_{ex}(14, 2+, A, HS)	E_{em}(14, 2+, A, LS)	E_{em}(14, 2+, A, HS)
$CsCaCl_3$:Yb^{2+}	25 200	23 430	24 320	22 600
$CsSrCl_3$:Yb^{2+}	25 870	23 760	24 720	22 880
$CsCaBr_3$:Yb^{2+}	25 270	23 600	24 310	22 630
$CsSrBr_3$:Yb^{2+}	26 060	23 700	24 550	22 780
$CsCaI_3$:Yb^{2+}	24 940	22 645	23 420	21 770
$CsSrI_3$:Yb^{2+}	25 020	22 650	23 480	21 490
	24 200		22 640	
Estimates from Eu^{2+} data				
$CsCaCl_3$:Yb^{2+}	25 260	23 330	24 260	22 330
$CsSrCl_3$:Yb^{2+}	25 390	23 460	24 440	22 510
$CsCaBr_3$:Yb^{2+}	25 460	23 530	24 380	22 450
$CsSrBr_3$:Yb^{2+}	25 900	23 970	24 480	22 550
$CsCaI_3$:Yb^{2+}	24 800	22 870	23 500	21 570
$CsSrI_3$:Yb^{2+}	24 220	22 290	23 130	21 200

$$E_{ex}(14, 2+, A, HS) = 34\,000\ cm^{-1} - D(2+, A) - 806.5\ cm^{-1} \quad (1)$$

$$E_{ex}(14, 2+, A, LS) = 35\,930\ cm^{-1} - D(2+, A) - 806.5\ cm^{-1} \quad (2)$$

$$E_{em}(14, 2+, A, HS) = E_{ex}(14, 2+, A, HS) - \Delta S(2+, A) \quad (3)$$

$$E_{em}(14, 2+, A, LS) = E_{ex}(14, 2+, A, LS) - \Delta S(2+, A) \quad (4)$$

where we used the notation introduced by Dorenbos[1,32] to keep the comparison simple. $D(2+, A)$ denotes the red-shift of the lowest excited 5d state with respect to its position in the free ion in a given compound A and the energy of 806.5 cm^{-1} takes into account that the barycenter of the 5d states of Yb^{2+} generally deviates by that value from the respective states in Eu^{2+}.[32] It should be noted that eqn (1) and (2) only allow the determination of the two lowest excitation energies (in the $^2F_{7/2}$, t_{2g} submanifold) where a highly dominant spin character can be assigned to the transitions.[36] $\Delta S(2+, A)$ denotes the Stokes shift determined for Eu^{2+} in the given compound A, which is assumed to be equal for Yb^{2+} in Dorenbos' model.[32]

Fig. 5 depicts a comparison of the emission and the lowest excitation energies of both the spin-allowed and spin-forbidden transitions of Yb^{2+} plotted against the average bond length[54–56] In the chlorides and bromides, a change from the Ca-based to the Sr-based compound leads to a larger average metal–ligand distance that induces a lower crystal field splitting. Hence, a blue-shift in both emission and excitation energies is observed.

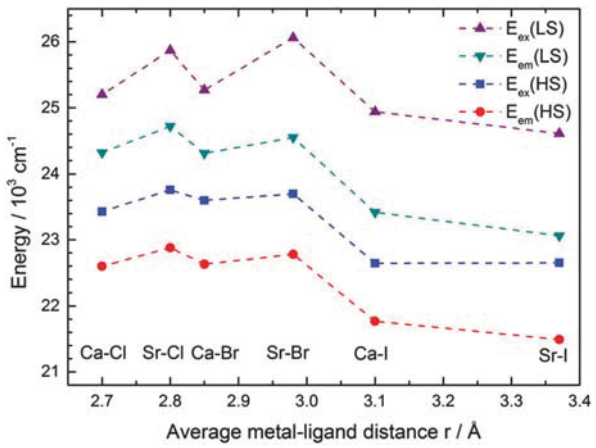

Fig. 5 Variation of the lowest excitation energies E_{ex}(LS), E_{ex}(HS) and the respective emission energies E_{em}(LS) and E_{em}(HS) of Yb^{2+} in $CsMX_3$ (M = Ca and Sr; X = Cl, Br, and I) dependent upon the average metal–ligand distance in the given compound.[54–56] For $CsSrI_3$, the detected excitation and emission energies of the LS transition were averaged.

Contrary to that, a change from chloride to heavier halide anions slightly increases the covalency and due to the nephelauxetic effect, a red-shift should be observed. This is particularly dominant upon change from a bromide to an iodide coordination sphere (see Fig. 5), in which the high difference in metal–ligand distances would actually lead to a blue-shift of the Yb^{2+} luminescence in the iodides if the crystal field had the dominant effect. Interestingly, the excitation and emission energies of the spin-allowed and spin-forbidden transitions of Yb^{2+} doped in $CsCaBr_3$ and $CsSrBr_3$ are almost equal to the energies found in the respective chlorides. This is easily explained by a compensating effect between covalency and the crystal field potential and indicates that both changes are of similar size within the transition from chlorides to bromides. Fig. 5 also reveals that the lowest excited states and the corresponding emission energies behave very much alike, which is a strong indication that the assignments are reasonable and the lowest excited states are in fact the emissive ones.

4.2 Effect of trigonal distortion in $CsSrI_3$:Yb^{2+}

$CsSrI_3$:Yb^{2+} plays a special role in this series, as we have already mentioned above. Although the energies of the two LS excitation and emission bands were averaged, respectively, a clear deviation from expectation can be observed as nearly all energies are red-shifted compared to those found in $CsCaI_3$:Yb^{2+} (the only exception being the spin-forbidden excitation $4f^{14}(^1S_0) \rightarrow 4f^{13}(^2F_{7/2})5d^1(t_{2g}, HS)$). This may be well understood taking into account the strong tilt of the $[SrI_6]^{4-}$ octahedra in the crystal structure of $CsSrI_3$ that leads to a non-negligible trigonal distortion from O_h to D_{3d} symmetry. We have discussed this effect very thoroughly for Eu^{2+} [52] and a clear analogy is found for Yb^{2+} as well.

One result of the trigonal distortion that leads to observable red-shifts in the spectra of Yb^{2+} requires the presence of symmetry-degenerate emissive states that split upon symmetry reduction. In the case of Eu^{2+}, this idea relates to a simple splitting of the t_{2g} crystal field states into a_{1g} and e_g states in D_{3d}.[52] In the case of Yb^{2+}, however, a more profound argument must be given.

Due to the relatively simple electronic structure of Yb^{2+} with only 140 microstates in the excited $4f^{13}5d^1$ configuration compared to Eu^{2+} with 30 030 microstates in its $4f^65d^1$ configuration, much more calculations are accessible to the former ion. For Eu^{2+}, it was recently shown that a ligand field theory-based DFT approach affords very reliable predictions for the excitation spectra in close agreement with experiment.[60,61] For Yb^{2+}, however, most of the first attempts used a strong-coupling scheme between the $4f^{13}$ core and the 5d electron embedded in a crystal field[19,20] in which the crystal field parameters were determined by least-squares fitting procedures. Most testing examples include host compounds with highly symmetric coordination environments such as MX:Yb^{2+} (M = Na and K; X = Cl, Br, and I),[24,64] $SrCl_2$:Yb^{2+} [22,33,34] or $CsCaBr_3$:Yb^{2+}.[35,36] In the latter two compounds, full-relativistic *ab initio* techniques were also employed that give rise to fully theoretical predictions of the absorption spectra of Yb^{2+} in these compounds.[33,35,36] For the case of $CsCaBr_3$:Yb^{2+}, however, the calculated emission and excitation energies are slightly blue shifted from our experimentally found values, which we mainly assign to the lower bond length the authors used in their calculation.[35,36]

One nice advantage of both the semi-empirical crystal field approach and the *ab initio* approach is that they allow a clear assignment of the crystal field states according to their Mulliken–Herzberg symbols. It turns out that the lowest spin-forbidden states mostly have triplet character and transform as into ^3E_u and $^3T_{2u}$ in octahedral symmetry, whereas the lowest spin-allowed state with singlet character transforms into $^1T_{1u}$.[25] It has been shown that these states are not completely pure in the sense that spin is no good quantum number anymore,[35,36] nonetheless this is a good approximation.

Our interpretation of the odd luminescence behavior of $CsSrI_3$:Yb^{2+} is depicted in a more detailed scheme in Fig. 6. The non-negligible trigonal distortion leads to a loss in degeneracy in both the spin-forbidden and spin-allowed states. Interestingly, the experimental spectra indicate that both final crystal field states $^1A_{2u}$ and ^1E_u are emissive thus giving rise to two spin-allowed emissions. This is easily understood in terms of symmetry selection rules since the transitions from both singlet states are spin- and symmetry-allowed in D_{3d} symmetry and hence should give rise to luminescence. The energetic order as shown in Fig. 6 may be justified in terms of the angular overlap model (AOM) and was discussed for the case of Eu^{2+}.[52] In the case of the spin-forbidden states, two effects have to be taken into account (see Fig. 6). The ^3E_u state retains its degeneracy upon trigonal distortion, whereas the $^3T_{2u}$ state splits into a $^3A_{1u}$ state and another ^3E_u state. From AOM considerations, the $^3A_{1u}$ state should lie lower in energy in complete analogy with the discussion to Eu^{2+}.[52] Due to the fact that two ^3E_u states of similar energies are now produced, perturbation according to the non-crossing rule is expected, which moreover leads to a shift in energy between the two ^3E_u states. It should be stressed that the initial ^3E_u state in O_h symmetry would have retained its energy otherwise upon distortion to D_{3d}. A clear hint on the energetic order of the HS states is

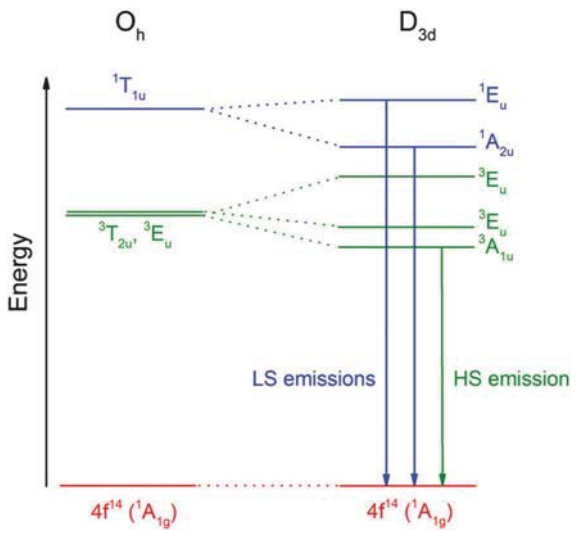

Fig. 6 Anticipated term scheme of Yb^{2+} doped in $CsSrI_3$, in which trigonal distortion takes place. The energies are not in scale and should only be taken qualitatively. For details, see text.

achievable by measurement of the decay time for the spin-forbidden transition in comparison to the other Sr-based halides, since the transition from the $^3A_{1u}$ state would be symmetry-forbidden in D_{3d}. This will be regarded by us in future. Unlike for the case of the spin-allowed transitions, other spin-forbidden transitions could not be resolved in the photoluminescence spectra of $CsSrI_3$:Yb^{2+} (see Fig. 4(b)). This model provides an explanation why most of the excitation and emission bands in $CsSrI_3$:Yb^{2+} are red-shifted compared to the doped Ca-analogue.

4.2 Fine structure of the excitation spectra

All photoluminescence excitation spectra exhibit a detailed fine structure that is much more complicated than known from Eu^{2+}-based excitation spectra. Parts of the bands may be grouped according to a decoupled scheme, in which the $4f^{13}$ core and the 5d electron are treated separately. Due to their shielded nature, the 4f electrons are treated as quasi-free and the states are hence denoted by their levels known from Yb^{3+} in the excited states, $^2F_{7/2}$ and $^2F_{5/2}$. The 5d orbitals, on the other hand, are highly prone to the local crystal field and hence give rise to the crystal field states t_{2g} and e_g in octahedral symmetry. This simple scheme, however, does not explain the rich fine structure of the separate groups of excitation bands. A very reasonable attempt has been given by Henke *et al.*[18,65] who took into account additional symmetry reductions that lead to a splitting in the t_{2g} and e_g states and explained the fine structure in the photoluminescence spectra of Yb^{2+}-doped fluorides by that. However, this approach would predict only two bands for each $4f^{13}(^2F_{7/2})5d^1(t_{2g})$, $4f^{13}(^2F_{5/2})5d^1(t_{2g})$ and $4f^{13}(^2F_{7/2})5d^1(e_g)$ submanifolds due to the exchange splitting into triplet and singlet states (see above) in perfect O_h symmetry. This is clearly not observed in the perovskite-like Yb^{2+}-doped hosts $CsCaCl_3$ and $CsCaBr_3$ (see Fig. 1(a) and 3(a)). Although phase transitions to lower-symmetric structures are reported for these two compounds at lower temperatures,[55,58] it may be assumed that this distortion is negligibly small, as has also been found for Eu^{2+} at 10 K.[51,52] Further evidence stems from the room temperature excitation spectra (not shown in this paper), in which the fine structure remains apart from worse resolution and where the $CsCaX_3$ (X = Cl and Br) compounds do have perfect perovskite structures. An insight into the observation of the complex fine structure is given taking into account the following Hamiltonian that describes the basic interactions of the 4f electrons and the 5d electron:[6]

$$\mathcal{H} = \mathcal{H}_{CF}(f) + \mathcal{H}_{CF}(d) + \mathcal{H}_{SO}(f) + \mathcal{H}_{SO}(d) + \mathcal{H}_{Coul}(fd) \quad (5)$$

with $\mathcal{H}_{CF}(f)$ and $\mathcal{H}_{CF}(d)$ as crystal field potentials acting on the 4f and 5d electrons, respectively, $\mathcal{H}_{SO}(f)$ and $\mathcal{H}_{SO}(d)$ as the Hamiltonians describing the spin–orbit interaction of the 4f and 5d electrons, respectively, and $\mathcal{H}_{Coul}(fd)$ as the Coulomb interaction between the 4f and 5d electrons. It should be noted that the Hamiltonian (5) is only correct for crystal fields with inversion symmetry, in which off-diagonal terms $\mathcal{H}_{CF}(fd)$ vanish. Within the decoupled scheme, the effects of spin–orbit coupling on the 5d electron, the crystal field potential acting on the 4f electrons as well as the Coulomb interaction between the $4f^{13}$ core and the 5d electron are neglected, which shows that it is a rather crude approximation. In particular, the last part of the Hamiltonian (5) is responsible for the detailed fine structure within one submanifold ($4f^{13}(^2F_{7/2})5d^1(t_{2g})$, $4f^{13}(^2F_{5/2})5d^1(t_{2g})$ or $4f^{13}(^2F_{7/2})5d^1(e_g)$) as well as the observation of the spin-forbidden and spin-allowed transitions for Yb^{2+}. A clear assignment of all states can only be attempted upon inclusion of the full Hamiltonian, as performed by the theoretical approaches mentioned above.[33,35,36,60,61] However, it becomes clear from the spectra that the decoupled scheme affords very reasonable results in a simple manner and without calculation, which is particularly important for experimentalists.

Interestingly, the occurrence of a detailed fine structure is obviously dependent on the type of surrounding ligands. Similarly fine-structured excitation spectra of Yb^{2+} are found for the doped alkali halides MX (M = Na and K; X = Cl, Br, and I)[24,64] or fluorides,[18,65] which is in good agreement with expectations and indicates that the ionic character of the Yb–ligand bond may play an important role in the observation of the fine structure in the excitation spectra. Another example that justifies this idea is found in the spectra of Yb^{2+}-doped CaS and SrS.[66] In these compounds, only three bands assigned to the different submanifolds as previously mentioned are observed in the photoluminescence excitation spectra and an electronic fine structure is absent. This may be related to the very soft character of sulfide ligands and hence, very covalent character of the Yb–S bond. Therefore, a strong covalency of the ligand field seems to quench the effect of the Coulomb interaction between the 4f and 5d electrons, which in turn influences the appearance of Yb^{2+}-based excitation or absorption spectra.

4.4 Effect on crystal field and exchange splitting

The crystal field splittings were also deduced for the Yb^{2+}-doped halides $CsMX_3$ (M = Ca and Sr; X = Cl, Br, and I). In spite of the fact that some of the regarded compounds do not provide

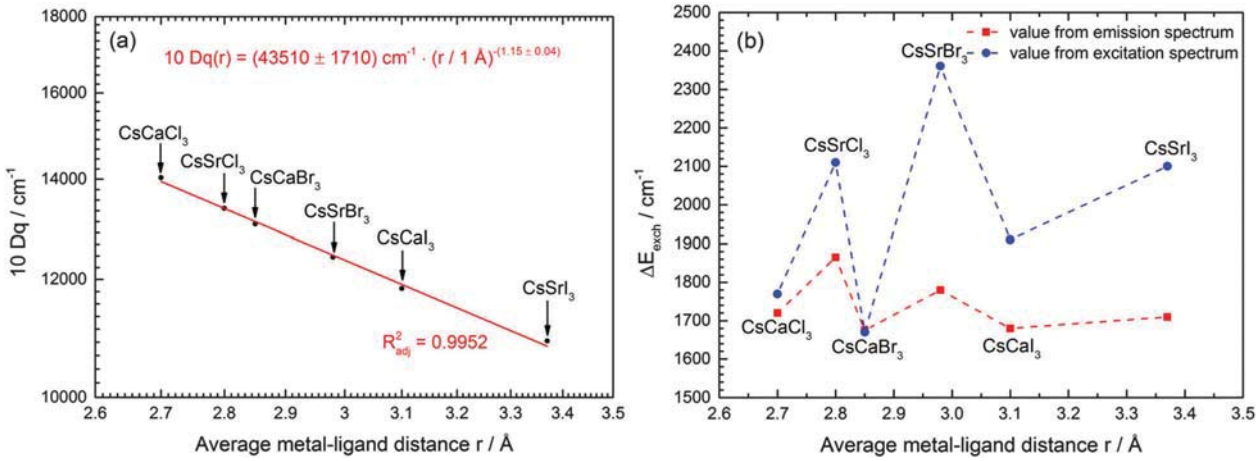

Fig. 7 Variation of (a) the determined crystal field splittings of 10 Dq (double-logarithmic scale) and (b) the exchange splittings between the spin-allowed and spin-forbidden transitions for Yb^{2+} determined from emission (red) and excitation (blue) spectra with the average metal–ligand distance r in $CsMX_3$ (M = Ca and Sr; X = Cl, Br, and I).[54–56]

perfect O_h-symmetric alkaline earth sites, the similar appearance of all excitation spectra as well as the interpretation within the decoupled scheme allows a reasonable estimation of the 10 Dq values. The clearest deviation from O_h symmetry is seen in the emission spectrum of $CsSrI_3$:Yb^{2+} (see Fig. 4(b)), which we have discussed above. Nonetheless, the very similar fine structure in the excitation spectrum provides a reasonable estimation for the 10 Dq value in terms of an undistorted crystal field. In all other compounds, the site symmetry can be well approximated by O_h symmetry, in accordance with our results found for Eu^{2+}.[51,52]

The relation of 10 Dq to the average metal–ligand distance provided in the given halides is depicted in Fig. 7 in a double-logarithmic scale. A remarkably good agreement with a power dependence on the metal–ligand distance is obtained, where we neglected severe changes in the bond length upon doping with Yb^{2+}, which is definitely fulfilled for the Ca-based halides due to the similarity of the ionic radii of Ca^{2+} and Yb^{2+}.[57] DFT-based cluster calculations recently showed that this is a reasonably good assumption even if the ionic radii of the alkaline earth and lanthanide ions differ a lot.[61,67] The dependence on the metal–ligand distance is weak compared to expectations from classical crystal field theory (r^{-5} dependence), but gets closer to the estimations of the chemical shift model of Dorenbos attempted for Ce^{3+} or Eu^{2+} (r^{-2} dependence).[68] We found an $r^{-1.2}$ dependence of 10 Dq of Yb^{2+} for the halides $CsMX_3$. All found crystal field splittings are slightly larger than the respective values reported for Eu^{2+}, which seems reasonable due to the smaller size of Yb^{2+} with respect to Eu^{2+} and the resulting shorter metal–ligand distance.[51,52,57] Nonetheless, the values of 10 Dq for both lanthanide ions are similar, which is a result of the weak dependence on the metal–ligand distance. Another confirmation that the deduced values are similar are provided by the reported results for the absorption spectra of Tm^{2+}-doped $CsCaX_3$ (X = Cl, Br, and I) that also lie in a similar range[6] except for $CsCaI_3$. We assign the deviation to the fact that the reported results for Tm^{2+} were determined for doping concentrations as large as 1 mol%, which decrease the resolution even at 10 K and lead to higher errors in the determination of 10 Dq. Moreover, calculated values of 10 Dq for the Yb^{2+}-doped alkali halides MX (M = Na and K; X = Cl, Br, and I) also fit nicely into expectations according to the similar bond lengths especially concerning the similar ionic radii of Na^+ and Ca^{2+}.[24,57,64]

Finally, the exchange splitting between the spin-forbidden and spin-allowed states is discussed. Due to the well-resolved spectra at 10 K, it was possible to determine the energy gap between the LS and HS states (see Tables 1–3) from both emission and excitation spectra with high accuracy. Their variation with the average metal–ligand distance is depicted in Fig. 7(b). For $CsSrI_3$, the position of the LS state was corrected for trigonal distortion to keep the exchange splitting comparable to the other compounds. It is evident that the exchange splitting is in general larger for the Sr-based halides than for the respective Ca-based ones and implies that a larger cation site induces a larger energy difference between the two emissive states. This coincides with the reported observations in literature so far, as a similar behavior can be noticed when regarding NaCl:Yb^{2+} (ΔE_{exch} = 1960 cm^{-1})[25] and $SrCl_2$:Yb^{2+} (ΔE_{exch} = 2090 cm^{-1}).[20,21] A clear variation with the covalency can, however, not be observed. In fact, the differences between the exchange splittings upon variation of the anion only are by far not as large as upon change of the cation, which implies that covalency does not have a comparably severe effect on the exchange splitting. This becomes particularly clear if the exchange splittings are determined from the emission spectra. Our results are in contradiction to the results reported for Tb^{3+},[69] where it was stated that an increase in covalency should lead to a decrease in exchange splitting due to higher spin admixture. We assume that the covalency within these halides does not vary as much as yielding a clear observable effect. Another clear feature evident from Fig. 7(b) is the difference in the values of exchange splittings determined from emission and excitation spectra. This is clearly related to the Stokes shifts. The analysis of the photoluminescence spectra reveals that the Stokes shifts for the HS and LS transitions are not always equal, respectively, especially if the

symmetry shows a larger deviation from perfect octahedral symmetry O_h (see Tables 1–3). This is particularly true for the Sr-based halides, which is also expected since the mismatch in ionic radii between Yb^{2+} and Sr^{2+} should lead to a slight symmetry distortion at least. Obviously, such a distortion leads to slightly different bond lengths in the HS and LS states. It is expected that this effect is directly reflected in the decay times of the spin-allowed and spin-forbidden transitions. From the recorded spectra, it turns out that the Stokes shift for the spin-allowed transition is generally larger than for the respective spin-forbidden transition in those halides, in which a higher deviation from O_h symmetry is expected. This indicates a larger amount of reorganization of electron density in the excited state if the symmetry is lower. For the Ca-based halides, however, the deviation of the exchange splittings determined from emission and excitation spectra is much lower indicating a much more symmetric arrangement for Yb^{2+}. Fig. 7(b) nicely illustrates that both emission and excitation spectra are important for a clear discussion on the exchange splittings. The determination from the excitation spectra is basically limited by the resolution and highly depends on factors like concentration, temperature and the local crystal field.[32]

5 Conclusions

The photoluminescence spectra of Yb^{2+} in the perovskite-analogues $CsMX_3$ (M = Ca and Sr; X = Cl, Br, and I) were analyzed. Yb^{2+} exhibits two types of emissions located in the violet and blue range in these compounds, respectively. The red-shifted emission is assigned to a spin-forbidden or HS-type transition, whereas the higher energetic emission can be interpreted as a spin-allowed or LS-type transition. The excitation spectra provide a characteristic well-resolved fine structure that can be partly interpreted in terms of a decoupled scheme, which neglects Coulomb interactions between the $4f^{13}$ core and the $5d^1$ electron. Within this approximation, it is already possible to group several bands into the submanifolds $4f^{13}(^2F_{7/2})5d^1(t_{2g})$, $4f^{13}(^2F_{5/2})5d^1(t_{2g})$ and $4f^{13}(^2F_{7/2})5d^1(e_g)$. The additional fine structure within each of these submanifolds, however, already indicates the limits of this scheme and can only be appropriately interpreted in terms of a full interaction Hamiltonian, *i.e.* by calculation. Reasonable values for the crystal field splitting, 10 Dq, are found that are in agreement with expectations concerning covalency (change of the anion) and metal–ligand distances (change of the cation). It turns out that they obey a power dependence on the metal–ligand distance, which is much weaker than expected by simple crystal field theory. They also lie in reasonable order upon comparison with the values known from Eu^{2+}. It is found that the spectroscopic properties of Eu^{2+} in the presented host compounds allow a very accurate estimation of the respective emission and excitation energies of Yb^{2+} in the same compounds.

$CsSrI_3$:Yb^{2+} takes a special role in the series of halido-perovskites as the crystal structure induces a trigonal distortion on the Yb^{2+} ions and hence exhibits two spin-allowed emission bands at low temperatures. Moreover, this model explains why the emissions are slightly red-shifted compared to the Ca analogue.

Finally, the exchange splittings between the LS and HS states were analyzed. It increases upon increase of the size of the alkaline earth site, whereas no clear and significant trend is observed for a change of the anion. Moreover, it was shown that its magnitude depends on the relative behavior of the Stokes shifts of the LS and HS transitions and hence, a difference in the values determined from emission or excitation spectra may occur.

In summary, very clear structure–luminescence relationships are evident for Yb^{2+} in this series that can even be correlated to Eu^{2+}. The presented luminescence properties might be interesting for novel scintillating or luminescent materials in general as well as for basic considerations concerning divalent lanthanides beyond Eu^{2+}.

Acknowledgements

We thank John Hermann for the photographs of the luminescent samples and Dr Patrick Larsen for preliminary raw investigations.

Notes and references

1 P. Dorenbos, *J. Lumin.*, 2003, **104**, 239.
2 H. Terraschke and C. Wickleder, *Chem. Rev.*, 2015, **115**, 11352.
3 J. O. Rubio, *J. Phys. Chem. Solids*, 1991, **52**, 101.
4 C. Wickleder, *J. Alloys Compd.*, 2000, **300–301**, 193.
5 J. Grimm, J. F. Suyver, E. Beurer, G. Carver and H. U. Güdel, *J. Phys. Chem. B*, 2006, **110**, 2093.
6 J. Grimm, E. Beurer and H. U. Güdel, *Inorg. Chem.*, 2006, **45**, 10905.
7 O. S. Wenger, C. Wickleder, K. W. Krämer and H. U. Güdel, *J. Lumin.*, 2001, **294–295**, 101.
8 J. Grimm, E. Beurer, P. Gerner and H. U. Güdel, *Chem. – Eur. J.*, 2007, **13**, 1152.
9 D. McClure and C. Pédrini, *Phys. Rev. B: Condens. Matter Mater. Phys.*, 1985, **32**, 8465.
10 P. Dorenbos, *J. Phys.: Condens. Matter*, 2003, **15**, 2645.
11 P. S. Senanayake, J.-P. R. Wells, M. F. Reid, G. Berden and A. Meijerink. R. J. Reeves, *Appl. Phys. Lett.*, 2012, **100**, 041902.
12 P. S. Senanayake, J.-P. R. Wells, M. F. Reid, G. Berden, A. Meijerink and R. J. Reeves, *J. Lumin.*, 2013, **133**, 81.
13 Z. Barandiarán and L. Seijo, *J. Chem. Phys.*, 2014, **141**, 234704.
14 R. T. Wegh and A. Meijerink, *Phys. Rev. B: Condens. Matter Mater. Phys.*, 1999, **60**, 10820.
15 L. van Pieterson, R. T. Wegh, A. Meijerink and M. F. Reid, *J. Chem. Phys.*, 2001, **115**, 9382.
16 L. van Pieterson, R. T. Wegh, A. Meijerink and M. F. Reid, *Phys. Rev. B: Condens. Matter Mater. Phys.*, 2002, **65**, 045114.
17 S. Lizzo, A. Meijerink, G. J. Dirksen and G. Blasse, *J. Lumin.*, 1995, **63**, 223.
18 S. Kück, M. Henke and K. Rademaker, *Laser Phys.*, 2001, **11**, 116.
19 E. Loh, *Phys. Rev.*, 1969, **184**, 348.

20 T. S. Piper, J. P. Brown and D. S. McClure, *J. Chem. Phys.*, 1967, **46**, 1353.
21 E. Loh, *Phys. Rev. B: Solid State*, 1973, **7**, 1846.
22 Z. Pan, C. Duan and P. A. Tanner, *Phys. Rev. B: Condens. Matter Mater. Phys.*, 2008, **77**, 085114.
23 W. J. Schipper and G. Blasse, *J. Solid State Chem.*, 1991, **94**, 418.
24 S. W. Bland and M. J. A. Smith, *J. Phys. C: Solid State Phys.*, 1985, **18**, 1525.
25 T. Tsuboi, D. S. McClure and W. C. Wong, *Phys. Rev. B: Condens. Matter Mater. Phys.*, 1993, **48**, 62.
26 G. Blasse, G. J. Dirksen and A. Meijerink, *Chem. Phys. Lett.*, 1990, **167**, 41.
27 V. P. Dotsenko, I. V. Berezovskaya, P. V. Pyrogenko, N. P. Efryushina, P. A. Rodnyi, C. W. E. van Eijk and A. V. Sidorenko, *J. Solid State Chem.*, 2002, **166**, 271.
28 S. Lizzo, A. Meijerink and G. Blasse, *J. Lumin.*, 1994, **59**, 185.
29 S. Lizzo, E. P. K. Nagelvoort, R. Erens, A. Meijerink and G. Blasse, *J. Phys. Chem. Solids*, 1997, **58**, 963.
30 V. Bachmann, T. Jüstel, A. Meijerink, C. Ronda and P. J. Schmidt, *J. Lumin.*, 2006, **121**, 441.
31 Z. Zhang, O. M. ten Kate, A. C. A. Delsing, M. J. H. Stevens, J. Zhao, P. H. L. Notten, P. Dorenbos and H. T. Hintzen, *J. Mater. Chem.*, 2012, **22**, 23871.
32 P. Dorenbos, *J. Phys.: Condens. Matter*, 2003, **15**, 575.
33 G. Sánchez-Sanz, L. Seijo and Z. Barandiáran, *J. Chem. Phys.*, 2010, **133**, 114506.
34 G. Sánchez-Sanz, L. Seijo and Z. Barandiáran, *J. Chem. Phys.*, 2010, **133**, 114509.
35 G. Sánchez-Sanz, L. Seijo and Z. Barandiáran, *J. Chem. Phys.*, 2009, **131**, 024505.
36 G. Sánchez-Sanz, L. Seijo and Z. Barandiáran, *J. Phys. Chem. A*, 2009, **113**, 12591.
37 A. J. Salkeld, M. F. Reid, J.-P. R. Wells, G. Sánchez-Sanz, L. Seijo and Z. Barandiarán, *J. Phys.: Condens. Matter*, 2013, **25**, 415504.
38 S. Lizzo, A. Meijerink, G. J. Dirksen and G. Blasse, *J. Phys. Chem. Solids*, 1995, **56**, 959.
39 J. R. Raipurkar, R. G. Atram, P. L. Muthal, S. M. Dhopte and S. V. Moharil, *J. Lumin.*, 2013, **134**, 456.
40 X. Zhao, Y. Deng, Z. Li and S. Wang, *J. Alloys Compd.*, 1997, **250**, 405.
41 E. Rowe, P. Bhattacharya, E. Tupitsyn, M. Groza, A. Burger, N. J. Cherepy, S. A. Payne, B. W. Sturm and C. Pédrini, *IEEE Trans. Nucl. Sci.*, 2013, **60**, 1057.
42 Y. Wu, G. Ren, M. Nikl, X. Chen, D. Ding, H. Li, S. Pana and F. Yang, *CrystEngComm*, 2014, **16**, 3312.
43 M. Alekhin, D. A. Biner, K. W. Krämer and P. Dorenbos, *Opt. Mater.*, 2014, **37**, 382.
44 M. Zhuravleva, B. Blalock, K. Yang, M. Koschan and C. L. Melcher, *J. Cryst. Growth*, 2012, **352**, 115.
45 M. Tyagi, M. Zhuravleva and C. L. Melcher, *J. Appl. Phys.*, 2013, **113**, 203504.
46 V. L. Cherginets, A. Y. Grippa, T. P. Rebrova, Y. N. Datsko, T. V. Ponomarenko, N. V. Rebrova, N. N. Kosinov, O. A. Tarasenko, Y. I. Dolzhenko and O. V. Zelenskaya, *Funct. Mater.*, 2012, **19**, 187.
47 A. Yu. Grippa, N. V. Rebrova, T. E. Gorbacheva, V. Y. Pedash, N. N. Kosinov, V. L. Cherginets, V. A. Tarasov, O. A. Tarasenko and A. V. Lopin, *J. Cryst. Growth*, 2013, **371**, 112.
48 V. L. Cherginets, A. Y. Grippa, T. P. Rebrova, Y. N. Datsko, T. V. Ponomarenko, N. V. Rebrova, N. N. Kosinov and O. V. Zelenskaya, *Funct. Mater.*, 2012, **19**, 429.
49 K. Yang, M. Zhuravleva and C. L. Melcher, *Phys. Status Solidi RRL*, 2011, **5**, 43.
50 D. H. Gahane, N. S. Kokode, B. M. Bahirwar and S. V. Moharil, *Phys. Procedia*, 2012, **29**, 42.
51 M. Suta, P. Larsen, F. Lavoie-Cardinal and C. Wickleder, *J. Lumin.*, 2014, **149**, 35.
52 M. Suta and C. Wickleder, *J. Mater. Chem. C*, 2015, **3**, 5233.
53 J. K. Howell and L. L. Pytlewski, *J. Less-Common Met.*, 1969, **18**, 437.
54 H. F. McMurdie, J. de Groot, M. Morris and H. E. Swanson, *J. Research NBS*, 1969, **73A**, 621.
55 H. J. Seifert and D. Haberhauer, *Z. Anorg. Allg. Chem.*, 1982, **491**, 301.
56 G. Schilling and G. Meyer, *Z. Anorg. Allg. Chem.*, 1996, **622**, 759.
57 R. D. Shannon, *Acta Crystallogr., Sect. A: Cryst. Phys., Diffr., Theor. Gen. Crystallogr.*, 1976, **32**, 751.
58 H.-J. Seifert and D. Haberhauer, *Z. Anorg. Allg. Chem.*, 1969, **368**, 36.
59 F. M. Ryan, W. Lehmann, D. W. Feldman and J. Murphy, *J. Electrochem. Soc.*, 1974, **121**, 1475.
60 A. García-Fuente, F. Cimpoesu, H. Ramanantoanina, B. Herden, C. Daul, M. Suta, C. Wickleder and W. Urland, *Chem. Phys. Lett.*, 2015, **622**, 120.
61 H. Ramanantoanina, F. Cimpoesu, C. Göttel, M. Sahnoun, B. Herden, M. Suta, C. Wickleder, W. Urland and C. Daul, *Inorg. Chem.*, 2015, **54**, 8319.
62 G. H. Dieke, in *Spectra and Energy Levels of Rare Earths in Crystals*, ed. H. M. Crosswhite and H. Crosswhite, Wiley, New York, 1968.
63 T. Tsuboi, H. Witzke and D. S. McClure, *J. Lumin.*, 1981, **24/25**, 305.
64 C.-K. Duan and P. A. Tanner, *J. Phys.: Condens. Matter*, 2008, **20**, 215228.
65 M. Henke, *Interkonfigurale Übergänge Lanthanid-dotierter Kristalle*, PhD thesis, University of Hamburg, 2001.
66 A. B. Parmentier, J. J. Joos, P. F. Smet and D. Poelman, *J. Lumin.*, 2014, **154**, 445.
67 H. Ramanantoanina, W. Urland, B. Herden, F. Cimpoesu and C. Daul, *Phys. Chem. Chem. Phys.*, 2015, **17**, 9116.
68 P. Dorenbos, *J. Phys.: Condens. Matter*, 2003, **15**, 4797.
69 P. Dorenbos, *J. Phys.: Condens. Matter*, 2003, **15**, 6249.